

## Self-Assembling Fullerenes for Improved Bulk-Heterojunction Photovoltaic Devices

Robert D. Kennedy, Alexander L. Ayzner, Darcy D. Wanger, Christopher T Day, Merissa Halim, Saeed I. Khan, Sarah H. Tolbert,\* Benjamin J. Schwartz,\* and Yves Rubin\*

Department of Chemistry and Biochemistry, University of California, Los Angeles, California 90095-1569

Received September 26, 2008; E-mail: tolbert@chem.ucla.edu; schwartz@chem.ucla.edu; rubin@chem.ucla.edu

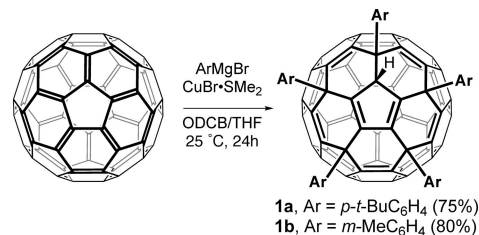
The recent dramatic increase in the cost of fossil fuels has generated a strong resurgence of interest in renewable solar energy sources. Although highly efficient, inorganic photovoltaic devices are costly. Advances in organic “bulk heterojunction” (BHJ) photovoltaic cells have opened prospects for the development of less expensive, easily produced alternatives.<sup>1</sup> To date, the efficiencies of organic BHJ cells have reached 5–6%, still short of the *ca.* 10% required for commercialization.<sup>2</sup>

The most efficient BHJ devices have been based on conjugated semiconducting polymers blended with a fullerene derivative that serves as an electron acceptor to split excitons created when the polymer absorbs light. These two components must be mixed together on a length scale that is shorter than the exciton diffusion length, typically *ca.* 10 nm, to ensure that all excitons are harvested.<sup>1</sup> It is also necessary that the polymer and fullerene components form a bicontinuous interpenetrating network for efficient carrier transport of the separated charges. Creating an optimal BHJ is a delicate balancing act: having the components blended too well prevents the formation of separate polymer and fullerene networks, but too much phase segregation leads to the formation of unconnected islands that can act as carrier traps. Indeed, low carrier mobilities in BHJ networks remain the major obstacle for improving device efficiency.<sup>1</sup> Thus, the key to improving BHJ devices is controlling the nanometer-scale morphology of the interpenetrating organic networks.

Several groups have presented methods for controlling the nm-scale morphology of polymer/fullerene blends based on macroscopic device-processing conditions. These include thermal annealing,<sup>3</sup> solvent-vapor treatments,<sup>4</sup> and the use of solvent additives that preferentially dissolve the fullerene.<sup>5</sup> Here, we propose a molecular approach to the control of both the length-scale of polymer/fullerene phase segregation and the electron mobility in the fullerene network. Our method is based on replacing conventional fullerene electron acceptors, such as [6,6]-phenyl-C<sub>61</sub>-butyric acid methyl ester (PCBM), with self-assembling fullerene derivatives that may form one-dimensional (1-D) wire-like domains within the active layer. Specifically, we examine a pair of fullerene derivatives that are chemically nearly identical (**1a** and **1b**) but whose molecular shapes either promote or hinder the formation of 1-D stacks. We find that even with identical processing conditions, the nonstacking fullerene **1b** gives poor performance in solar cells based on blends with regioregular poly(3-hexylthiophene-2,5-diyl) (P3HT) but that the stacking fullerene **1a** leads to enhanced photovoltaic efficiency.

The new fullerene adducts **1a** and **1b** are related to those synthesized by Nakamura and co-workers, who have developed a highly regioselective and efficient penta-addition of aryl copper reagents to C<sub>60</sub> that produces molecules with “shuttlecock”-like shapes (Scheme 1).<sup>6</sup> An intriguing feature of these molecules is that some of them tend to form columnar motifs in the solid state,<sup>7</sup> in which the curved surface of one fullerene nestles inside the cavity

Scheme 1



produced by the five arms of the adjacent molecule. In a future study of the crystal structures of 20 of these adducts, we will show that modification of the substituent arms allows control over their propensity for stacking. Here we focus on BHJ solar cells prepared from **1a** and **1b**, with the goal of understanding how molecular control over fullerene–fullerene interactions might translate into a more favorable BHJ morphology and thus improve electron mobility and photovoltaic device performance.

The molecular design of fullerene shuttlecock adducts for use in BHJ solar cells is challenging for a number of reasons: the fullerene molecules must have a propensity to self-assemble into desirable structures and display high solubility in solvents used for device fabrication, two properties that are often mutually exclusive. To determine the optimal geometry of a shuttlecock that is likely to stack efficiently with short fullerene–fullerene contact distances, we performed a series of molecular modeling calculations (AM1, Spartan 04). These calculations indicated that the introduction of the large *tert*-butyl group at the *para*-position of each of the phenyl substituents produces a deep, well-shaped cavity that should promote self-assembly. We thus synthesized compound **1a** and found that the addition of the *para tert*-butyl groups makes **1a** an efficient self-assembling 1-D “stacker” that also is suitably soluble in *o*-dichlorobenzene (ODCB).

Following the general procedure of Nakamura et al.,<sup>6,8</sup> **1a** was obtained as a bright red solid and purified by column chromatography on silica gel. Figure 1 shows the X-ray structure of **1a**·(C<sub>5</sub>H<sub>12</sub>)<sub>3</sub> obtained by slow diffusion of *n*-pentane into a saturated solution of **1a** in 1-chloronaphthalene.<sup>9</sup> In this structure, the fullerenes form 1-D stacks that are aligned antiparallel and separated by sheaths of *n*-pentane molecules. The distance between fullerene centroids within each column is 10.83 Å, and the shortest distances between fullerene centroids in adjacent columns are 14.85 and 15.86 Å.

We also examined the crystal structures of **1a** crystallized from ODCB, CS<sub>2</sub>, and C<sub>6</sub>H<sub>5</sub>Cl and found **1a** is a “universal stacker”: crystals of **1a** display a packing motif characterized by the assembly of 1-D fullerene stacks that is solvent-independent.<sup>8</sup> For the four solvents we examined, it appears that the overall packing structure is dictated by the self-assembly of the 1-D stacks and that the solvent molecules simply fill in the voids.

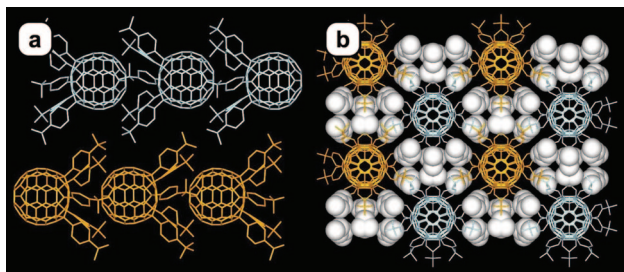


**Figure 1.** Crystal structure of **1a**·( $C_5H_{12}$ )<sub>3</sub>. (a) Antiparallel *a*-axis stacks, viewed along the (a) *bc* plane and (b) *a*-axis. Hydrogens are removed for clarity; *n*-pentane solvent molecules are shown in space-filling mode.

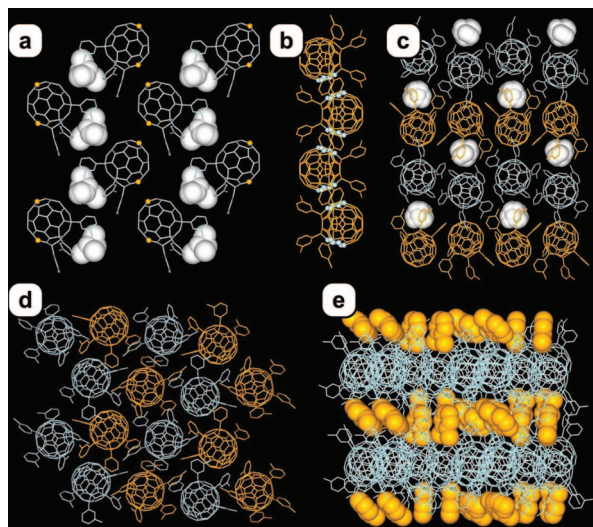


**Figure 2.** Crystal structure of **1b**· $CHCl_3$ . (a) *ac* layer, viewed along the *b* axis, with disordered  $CHCl_3$  solvent shown in space-filling representation. (b) Single *b*-axis chain, viewed along the *a* axis. Carbon atoms with close contacts (3.412–3.551 Å) are highlighted. (c) Crystal structure of **1b**·( $C_6H_5Cl$ )<sub>1.875</sub>. Single *bc* layer, viewed along the *a* axis, with selected solvent molecules shown in space-filling representation. (d) Crystal structure of **1b**· $C_6H_4Cl_2$ . Single *bc* layer, viewed along the *a* axis, with the solvent removed for clarity. (e) *bc* Layers for **1b**· $C_6H_4Cl_2$  viewed along the *b* axis, with solvent molecules shown in space-filling representation. Hydrogen atoms are removed for clarity in all structures above.

Because the reduction of the local symmetry of a group tends to increase overall molecular solubility, we also investigated the 3-tolyl system **1b**: the solubility of this molecule in ODCB is *ca.* 10 mg/mL, which is high enough for the ready fabrication of devices by spin-coating from a concentrated solution of this fullerene mixed with **P3HT**. Crystals suitable for single-crystal X-ray diffraction were grown from five different solvent systems, resulting in very different extended crystal structures.<sup>10</sup> Figure 2a,b shows the packing structure of compound **1b**· $CHCl_3$  grown from a concentrated solution in a  $CHCl_3/CS_2$  mixture. The chloroform molecules reside just within the cavity formed by the five *meta*-tolyl groups, and the fullerene-solvent units form a close-packed 3-D diamond-like network in which each fullerene has four near-neighbors arranged in an approximately tetrahedral geometry. The fullerene centroid–centroid distances are 10.436 (edge–vertex close contacts, Figure 2a) and 9.894 Å (hexagon–hexagon, Figure 2b), respectively. An identical motif is observed in the crystal structure of **1b**· $CS_2$ , grown by slow diffusion of *n*-pentane into a  $CS_2$  solution of **1b**. In contrast, **1b**·**1,2- $C_6H_4Cl_2$**  (Figure 2d,e) forms a layered structure.<sup>10</sup> Although the cocrystallized ODCB molecules reside just within the cavity in a similar fashion to **1b**· $CHCl_3$ , alternating layers of fullerene and solvent are observed with a periodicity of

16.55 Å (Figure 2e). The fullerenes within each layer are roughly hexagonally packed, and each fullerene has five near-neighbors ( $C_{60}$  centroid–centroid distances  $\leq 10.193$  Å). Nearly identical packing is observed for **1b**· $C_6H_5CH_3$  (slow evaporation of  $PhCH_3$ ).<sup>10</sup> However, the crystal structure of **1b**·( $C_6H_5Cl$ )<sub>1.875</sub> is very different, with each fullerene having three near-neighbors ( $C_{60}$  centroid–centroid distances  $\leq 10.318$  Å), forming a layered, puckered, honeycomb network (Figure 2c).<sup>10</sup> These diverse structures make it clear that **1b** does not tend to form 1-D stacks, so we shall use it as a model nonstacking shuttlecock.

Clearly, the packing of **1a** contrasts greatly with that of **1b**, in which subtle changes in the solvent produced entirely different structural motifs. The difference can be rationalized on the basis of molecular shape: the deeper cavity of **1a** resulting from *para*-substitution promotes efficient 1-D stacking, while the *meta*-substituted phenyl arms of **1b** produce only a shallow cavity.

An ideal BHJ solar cell should have two networks that are both continuous and fully interconnected throughout the thickness of the active layer. For polymer/fullerene-based BHJ solar cells, a fullerene derivative with a propensity to form 1-D stacks may form a more ideal network than one that makes isotropic aggregates that could more easily lead to island formation. To test this idea, we fabricated BHJ solar cells from blends of either **1a** or **1b** with **P3HT**.<sup>8</sup> Although we do not necessarily expect these blends to contain fullerene aggregates with structures identical to those shown in Figures 1 and 2, it seems likely that the robust stacking and nonstacking molecular motifs found in the single crystals also will be present in the devices.

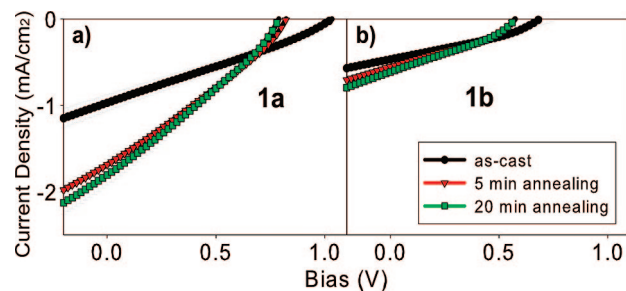


**Figure 3.** (a) *I*–*V* curves for as-cast and thermally annealed BHJ solar cells made from a 1:0.35 blend of **1a** and **P3HT**. Annealing of these cells also occurs rapidly, with significantly improved device efficiencies compared to the data in (b). (b) *I*–*V* curves for as-cast and thermally annealed BHJ solar cells made from a 1:0.45 blend of **1b** and **P3HT**. Annealing of these cells is complete in 5 min, but the overall device performance is low.

A comparison between the current density–voltage (*I*–*V*) characteristics of as-cast **P3HT:1a** and **P3HT:1b** devices<sup>11</sup> under simulated AM1.5 solar irradiation<sup>8</sup> is shown in Figure 3a,b. The *I*–*V* curves show that both the short-circuit current density ( $I_{sc}$ ) and open-circuit voltage ( $V_{oc}$ ) are larger for the devices fabricated with **1a**. The larger value of  $I_{sc}$  for **1a** is consistent with the idea of this stacking shuttlecock producing a more interconnected network compared to **1b**. The difference in  $V_{oc}$  is less straightforward to interpret. The value of  $V_{oc}$  is thought to depend only on the difference of the donor HOMO and acceptor LUMO energies,<sup>12</sup> but these devices use the same donor and the LUMO levels of **1a** and **1b** are nearly identical. Thus, the difference must be related to the nm-scale morphology of the fullerene network. One explanation is that the different fullerene networks have different densities of charge-carrier traps, which contribute to the space-charge buildup and thus affect the built-in potential in the device. Alternatively, the different fullerene aggregation geometries may affect the self-organization and/or crystallinity of the **P3HT**: a change in the

crystallinity or average conjugation length could be reflected in the spatially averaged HOMO of the polymer, thereby directly affecting  $V_{oc}$ .

Since thermal annealing frequently improves the efficiency of polymer-based BHJ solar cells, we chose to anneal our solar cells based on blends of **P3HT** with **1a** or **1b** under conditions similar to those used to improve the efficiency of **P3HT:PCBM** solar cells.<sup>3</sup> As with **P3HT:PCBM** devices, annealing our devices based on **1a** and **1b** decreased  $V_{oc}$  but increased  $I_{sc}$ , leading to an overall increase in efficiency (Figure 3). The reduction in  $V_{oc}$  is generally assigned to reduced space-charge buildup while the increase in  $I_{sc}$  is related to improved network formation. We find that the annealing-induced increase in  $I_{sc}$ , which is the most direct indicator of the underlying network structure, is less than half as large for **1b** compared to **1a**. Since the electronic structures of these two fullerenes are essentially identical, the larger improvement in photovoltaic performance upon annealing devices based on *tert*-butyl system **1a** must be associated with the increased self-organization of this fullerene derivative.

Thermal annealing is a kinetically slow process that requires the diffusive motion of molecules. Indeed, **P3HT:PCBM** devices show a steady improvement in performance with thermal annealing for *ca.* 20 min, after which time the performance plateaus.<sup>3</sup> This large improvement does not occur for devices that have been subjected to “solvent annealing” by casting from slow-evaporating solvents such as ODCB.<sup>4</sup> In contrast, we find that thermal annealing has a pronounced effect on shuttlecock-based devices cast out of ODCB. Moreover, this thermally induced improvement occurs quickly: for devices based on both **1a** and **1b**, no further improvement in the photovoltaic efficiency is produced past 5 min of annealing (Figure 3a,b). We also find that device performance is relatively insensitive to the amount of **1a** but depends critically on the concentration of **PCBM**.<sup>3</sup> This indicates that there are qualitative differences in both the degree and nature of the phase segregation for shuttlecock-based devices relative to photovoltaic devices based on the conventional **PCBM**.

The reason that thermal annealing improves the efficiency of polymer-based BHJ solar cells is still the subject of investigation: it is known that annealing increases the crystallinity of **P3HT**, thus improving the hole mobility in the device,<sup>13</sup> but the effects of annealing on the fullerene network are less clear. Annealing is known to promote phase segregation, which could either enhance electron mobility due to better fullerene–fullerene contacts<sup>14</sup> or decrease electron mobility as phase segregation produces islands within the fullerene network.<sup>11,15</sup> The strong propensity of **1a** to form 1-D stacks regardless of solvent conditions (Figure 1) suggests that this molecule may be less likely to form islands or other unconnected structures upon thermal annealing. In contrast, fullerenes like **1b** that tend to aggregate into more isotropic structures may promote the same type of undesirable phase segregation that is observed with traditional fullerene derivatives such as **PCBM**. Moreover, it is possible that the packing of the **P3HT** chains is strongly dependent on the nanometer-scale morphology of the fullerene derivative, so that the propensity of **1a** to stack in a columnar motif could be conducive to improved polymer  $\pi$ – $\pi$  interactions and thus lead to higher hole mobility.

We close by noting that the efficiency of the photovoltaic devices based on **1a** reaches up to *ca.* 1.5%, lower than the 5–6% achieved in devices based on **PCBM**.<sup>1,2</sup> Although our processing conditions (e.g., polymer–fullerene ratio, solvent, spin-coating conditions, etc.) will benefit from further optimization, we believe that a greater parameter to improve lies in the optimization of contacts between the fullerene moieties within the solid-state packing of the

shuttlecock molecules. **PCBM** has unusually short fullerene C–C contact distances, as observed in the crystal structures of **PCBM·PhCl** ( $\geq 2.902$  Å) and **PCBM·ODCB** ( $\geq 3.171$  Å); this high degree of contact should greatly favor electron mobility.<sup>16</sup> Even with the high propensity of **1a** to form columnar stacks, the closest fullerene–fullerene contacts in the crystal structures are relatively long ( $\geq 4.035$  Å, **1a·(C<sub>5</sub>H<sub>12</sub>)<sub>3</sub>**). We attribute this both to the repulsive interaction between *meta*-aryl hydrogens of the shuttlecock “feathers” with the neighboring fullerene ball, which prevents closer approach of molecules along the stacks, and to the interstack steric crowding by the “feathers” that keep individual columns well separated. The shuttlecock system, however, allows for incredible chemical diversity within a single molecular motif. We are thus currently exploring crystal structures and BHJ device behavior of a large range of penta-substituted fullerene derivatives with the goal of improving BHJ solar cell efficiency by simultaneously optimizing the propensity for fullerenes to stack, the fullerene–fullerene contact distances, and the degree of phase segregation with conjugated polymers.

**Acknowledgment.** This work was supported by research and instrumentation grants ((NSF-CHE-0527015 and ONR-N00014-04-1-0410; Y.R./B.S./S.T.), NSF-CHE-0617052 (Y.R.), NSF-CHE-9871332 (X-ray), and NSF-CHE-9974928 (NMR)).

**Supporting Information Available:** Experimental procedures, spectra and CIF files for **1a·(C<sub>5</sub>H<sub>12</sub>)<sub>3</sub>**, **1b·C<sub>6</sub>H<sub>5</sub>CH<sub>3</sub>**, **1b·(C<sub>6</sub>H<sub>5</sub>Cl)<sub>1.875</sub>**, **1b·1,2-C<sub>6</sub>H<sub>4</sub>Cl<sub>2</sub>**, **1b·CHCl<sub>3</sub>**, **1b·CS<sub>2</sub>**. This material is available free of charge via the Internet at <http://pubs.acs.org>.

## References

- Hoppe, H.; Saricifci, S. *J. Mater. Chem.* **2006**, *16*, 45–61.
- Li, G.; Shrotriya, V.; Yao, Y.; Huang, J.; Yang, Y. *J. Mater. Chem.* **2007**, *17*, 3126–3140.
- Ma, W.; Yang, C.; Gong, X.; Lee, K.; Heeger, A. *Adv. Funct. Mater.* **2005**, *15*, 1617–1622.
- Li, G.; Yao, Y.; Yang, H.; Shrotriya, V.; Yang, G.; Yang, Y. *Adv. Funct. Mater.* **2007**, *17*, 1636–1644.
- Lee, J. K.; Ma, W. L.; Brabec, C.; Yuen, J.; Moon, J. S.; Kim, J. Y.; Lee, K.; Bazan, G.; Heeger, A. *J. Am. Chem. Soc.* **2008**, *130*, 3619–3623.
- (a) Sawamura, M.; Iikura, H.; Nakamura, E. *J. Am. Chem. Soc.* **1996**, *118*, 12850–12851. (b) Sawamura, M.; Iikura, H.; Ohama, T.; Hackler, U. E.; Nakamura, E. *J. Organomet. Chem.* **2000**, *599*, 32–36. (c) Matsuo, Y.; Nakamura, E. *Chem. Rev.* **2008**, *108*, 3016–3028.
- (a) Sawamura, M.; Kawai, K.; Matsuo, Y.; Kanie, K.; Kato, T.; Nakamura, E. *Nature* **2002**, *419*, 703–705. (b) Zhong, Y.-W.; Matsuo, Y.; Nakamura, E. *Org. Lett.* **2006**, *8*, 1463–1466. (c) Zhong, Y.-W.; Matsuo, Y.; Nakamura, E. *J. Am. Chem. Soc.* **2007**, *129*, 3052–3053. (d) Matsuo, Y.; Tahara, K.; Morita, K.; Matsuo, K.; Nakamura, E. *Angew. Chem., Int. Ed.* **2007**, *46*, 2844–2847.
- See Supporting Information.
- X-ray data for **1a·(C<sub>5</sub>H<sub>12</sub>)<sub>3</sub>**: Red platelet ( $0.3 \times 0.2 \times 0.2$  mm<sup>3</sup>) from 1-chloronaphthalene/C<sub>5</sub>H<sub>12</sub>. Space group: *Pnma*;  $a = 21.661(3)$  Å;  $b = 22.721(4)$  Å;  $c = 17.128(3)$  Å;  $V = 8430(2)$  Å<sup>3</sup>;  $Z = 4$ ;  $T = 100(2)$  K;  $N_{ref}(\text{unique}) = 11\,521$ ;  $R_1 = 0.076$ ;  $R_w = 0.196$ .
- X-ray data for **1b·CHCl<sub>3</sub>**: red platelet ( $0.4 \times 0.1 \times 0.1$  mm<sup>3</sup>) from CHCl<sub>3</sub>/CS<sub>2</sub>. Space group: *Pnma*;  $a = 18.298(5)$  Å;  $b = 17.955(5)$  Å;  $c = 17.352(5)$  Å;  $V = 5701(3)$  Å<sup>3</sup>;  $Z = 4$ ;  $T = 100(2)$  K;  $N_{ref}(\text{unique}) = 7277$ ;  $R_1 = 0.077$ ;  $R_w = 0.200$ . **1b·CS<sub>2</sub>**: Red prism ( $0.2 \times 0.2 \times 0.05$  mm<sup>3</sup>) from CS<sub>2</sub>/C<sub>5</sub>H<sub>12</sub>. Space group: *Pnma*;  $a = 18.311(5)$  Å;  $b = 17.969(4)$  Å;  $c = 17.344(5)$  Å;  $V = 5707(3)$  Å<sup>3</sup>;  $Z = 4$ ;  $T = 100(2)$  K;  $N_{ref}(\text{unique}) = 7858$ ;  $R_1 = 0.063$ ;  $R_w = 0.171$ . For **1b·1,2-C<sub>6</sub>H<sub>4</sub>Cl<sub>2</sub>**, **1b·C<sub>6</sub>H<sub>5</sub>CH<sub>3</sub>**, and **1b·(C<sub>6</sub>H<sub>5</sub>Cl)<sub>1.875</sub>**, see Supporting Information.
- Ayzner, A. L.; Wanger, D. D.; Tassone, C. J.; Tolbert, S. H.; Schwartz, B. J. *J. Phys. Chem. C*, in press (ASAP available at, DOI: 10.1021/jp8076497).
- Branec, C.; Cravino, A.; Meissner, D.; Saricifci, S.; Fromherz, T.; Rispen, M.; Sanchez, L.; Hummelen, Y. *Adv. Funct. Mater.* **2001**, *11*, 374–380.
- Erb, T.; Zhokhavets, U.; Gobsch, G.; Raleva, S.; Stuhn, B.; Schilinsky, P.; Waldauf, C.; Brabec, C. *Adv. Funct. Mater.* **2005**, *15*, 1193–1196.
- Dante, M.; Peet, J.; Nguyen, T.-Q. *J. Phys. Chem. C* **2008**, *112*, 7241–7249.
- Warman, J.; de Haas, M. P.; Anthopoulos, T. D.; de Leeuw, D. M. *Adv. Mater.* **2006**, *18*, 2294–2298.
- Rispen, M. T.; Meetsma, A.; Rittberger, R.; Brabec, C. J.; Saricifci, N. S.; Hummelen, J. C. *Chem. Commun.* **2003**, 2116–2118.

JA807627U